AGU PUBLICATIONS

Tectonics

RESEARCH ARTICLE
10.1002/2016TC004147

Key Points:
- The Tanzanian basement rocks record two significant cooling events at 340–220 Ma and 70 Ma
- Cooling events in Tanzania are contemporaneous with subsidence histories of the Congo basin
- The cooling and subsidence events suggest complex regional geodynamics during the Phanerozoic

Correspondence to:
C. H. Kasanzu,
kcharls16@yahoo.com

Citation:
Kasanzu, C. H., B. Linol, M. J. de Wit, R. Brown, C. Persano, and F. M. Stuart (2016), From source to sink in central Gondwana: Exhumation of the Precambrian basement rocks of Tanzania and sediment accumulation in the adjacent Congo basin, *Tectonics*, *35*, doi:10.1002/2016TC004147.

Received 3 FEB 2016
Accepted 10 AUG 2016
Accepted article online 13 AUG 2016

From source to sink in central Gondwana: Exhumation of the Precambrian basement rocks of Tanzania and sediment accumulation in the adjacent Congo basin

Charles Happe Kasanzu[1], Bastien Linol[2,3], Maarten J. de Wit[3], Roderick Brown[4], Cristina Persano[4], and Finlay M. Stuart[5]

[1]Geology Department, University of Dar es Salaam, Dar es Salaam, Tanzania, [2]Department of Geosciences, Nelson Mandela Metropolitan University, Port Elizabeth, South Africa, [3]AEON-ESSRI, Nelson Mandela Metropolitan University, Port Elizabeth, South Africa, [4]School of Geographical and Earth Sciences, University of Glasgow, Glasgow, UK, [5]Scottish Universities Environmental Research Centre, East Kilbride, UK

Abstract Apatite fission track (AFT) and (U-Th)/He (AHe) thermochronometry data are reported and used to unravel the exhumation history of crystalline basement rocks from the elevated (>1000 m above sea level) but low-relief Tanzanian Craton. Coeval episodes of sedimentation documented within adjacent Paleozoic to Mesozoic basins of southern Tanzania and the Congo basin of the Democratic Republic of Congo indicate that most of the cooling in the basement rocks in Tanzania was linked to erosion. Basement samples were from an exploration borehole located within the craton and up to 2200 m below surface. Surface samples were also analyzed. AFT dates range between 317 ± 33 Ma and 188 ± 44 Ma. Alpha (Ft)-corrected AHe dates are between 433 ± 24 Ma and 154 ± 20 Ma. Modeling of the data reveals two important periods of cooling within the craton: one during the Carboniferous-Triassic (340–220 Ma) and a later, less well constrained episode, during the late Cretaceous. The later exhumation is well detected proximal to the East African Rift (70 Ma). Thermal histories combined with the estimated geothermal gradient of 9°C/km constrained by the AFT and AHe data from the craton and a mean surface temperature of 20°C indicate removal of up to 9 ± 2 km of overburden since the end of Paleozoic. The correlation of erosion of the craton and sedimentation and subsidence within the Congo basin in the Paleozoic may indicate regional flexural geodynamics of the lithosphere due to lithosphere buckling induced by far-field compressional tectonic processes and thereafter through deep mantle upwelling and epeirogeny tectonic processes.

1. Introduction

Insights into the geodynamic interplay between hinterlands and depocenters can be gained through thermochronological and basin subsidence studies [e.g., *Weber et al*., 2004; *Tinker et al*., 2008; *Fan and Carrapa*, 2014]. In particular, apatite fission track and (U-Th)/He studies on crustal rocks can furnish important information on the chronology and rate of cooling, exhumation history, and approximate magnitudes of exhumation [e.g., *Gleadow and Brown*, 2000; *Ehlers and Farley*, 2003; *Donelick et al*., 2005; *Tinker et al*., 2008; *Kasanzu*, 2014; *Torres-Acosta et al*., 2015]. The application of low-temperature thermochronology of stable lithospheric blocks such as cratons has proved to be particularly important in detecting shallow thermotectonic processes that cannot be detected by other conventional isotopic approaches such as zircon U-Pb dating (e.g., Sao Francisco Craton, Brazil [*Harman et al*., 1998]; Canadian Shield [*Lorencak et al*., 2004]; Fennoscandian Shield [*Cederbom et al*., 2000; *Hendriks and Redfield*, 2005; *Kohn et al*., 2009]; Yilgarn Craton, Australia [*Weber et al*., 2005]; Ukrainian Craton [*Danišík et al*., 2008]; and Zimbabwe Craton [*Belton and Raab*, 2010]).

The topography of Africa is characterized by large basins and swells, and because the continent is completely surrounded by passive margins (Figure 1), this bimodal topography cannot be explained simply by orogenesis alone [e.g., *Burke*, 1996; *French and Romanowicz*, 2015; *de Wit*, 2007]. The Tanzanian Craton at 2.6–3.6 Ga [*Manya et al*., 2006; *Kabete et al*., 2012] comprises part of the East African Plateau (>1100 m above sea level) that stretches from Zambia northward to the Afar junction. It forms a 5000 km long elevated structure or "superswell" [*Nyblade and Robinson*, 1994; *Lithgow-Bertelloni and Silver*, 1998; *Gurnis et al*., 2000; *Wererante et al*., 2003; *Moucha and Forte*, 2011; *Wichura et al*., 2015; *O'Donnell et al*., 2013; *Torres-Acosta et al*., 2015].

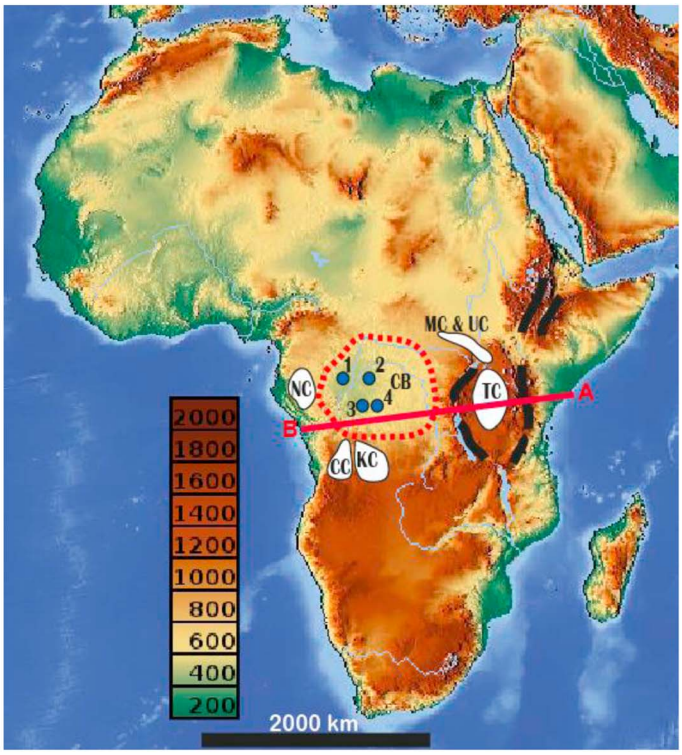

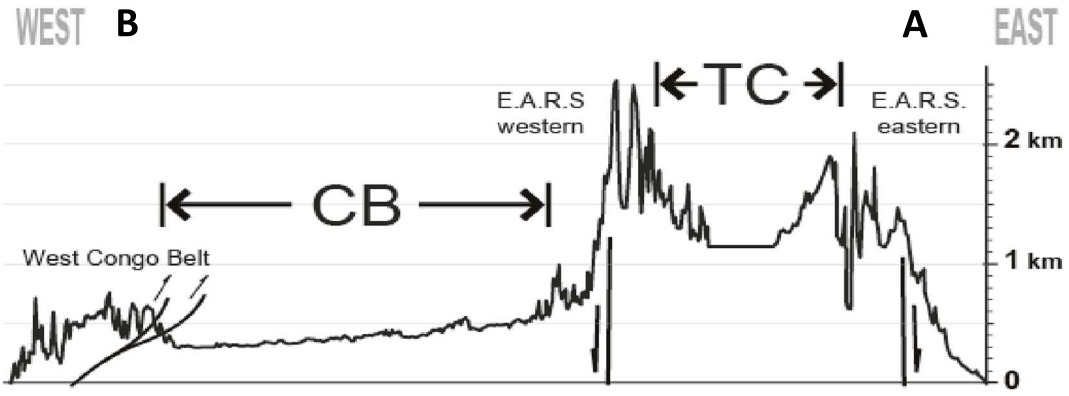

Figure 1. (top) Topography of Africa showing the highly elevated Eastern Africa plateau and the more subdued low-lying topography of central, west, and north Africa; the Congo basin (shown as CB) is marked by the thick dashed line (red); EARS is indicated by the thick black lines; Archean cratons are shown in white. (bottom) Cross section (A-B) across central Africa from the Indian to South Atlantic Oceans, across the Tanzanian Craton and the Congo basin to illustrate topographic contrast; NC = Ntem Craton; CC = Cuango Craton; KC = Kasai Craton; MC = Mboumou Craton; UC = Uganda Craton; TC = Tanzania Craton;. Locations of boreholes used from the Congo basin are shown in numbers (1 = Mbandaka, 2 = Samba, 3 = Gilson; 4 = Dekese).

This has been attributed to a mantle "hot spot" and convective upwelling beneath the African plate during the Neogene [*Nyblade and Brazier*, 2002; *Torres-Acosta et al*., 2015]. The Congo basin lies to the west of the craton. It covers about 10% by size of the African continent and marks a topographic low in sub-Saharan Africa [*Linol et al*., 2015a]. This topographic anomaly has been suggested to be related to an underlying "cold spot" and convective downwelling [see *Linol et al*., 2015c, and references therein]. Together, the Congo basin and the Tanzanian Craton are part of the Central African Shield (Figure 2) which is discussed in detail in *de Wit and Linol* [2015]. Other Precambrian terrains in the shield include the Ntem, Cuango, Kasai, Mboumou, and Uganda Cratons (Figure 1).

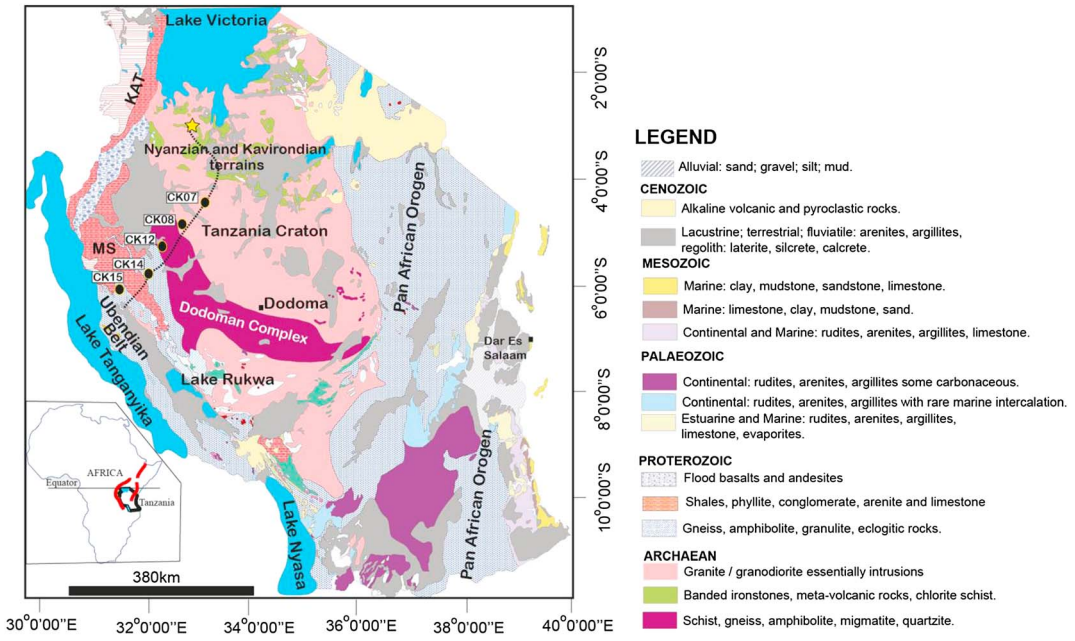

Figure 2. Simplified geological map of Tanzania showing craton and its other major tectonic terrains. The dotted black line indicates the transect of the present study, and the yellow star is the location of the sampled Bulyanhulu borehole. Surface samples locations and sample number are also shown. The lower left insert shows the geographical setting of Tanzania in Africa, with the EARS in thick red lines (modified from *Kasanzu* [2014]). KAT = Karagwe-Ankolean terrain.

Studies of the exhumation and subsidence histories in the region can provide a unique tectonic framework for the understanding of geodynamic linkages between hinterlands (used here to refer to sediment sources) and depocenters (used here to refer to sediment sinks). The apatite fission track (AFT) and (U-Th)/He (AHe) techniques record rock cooling between 110°C and 40°C and have been used extensively to place temporal constraints on ancient basement exhumation histories [e.g., *Brown et al*., 1994; *Tinker et al*., 2008; *Farley*, 2002; *Ehlers and Farley*, 2003; *Donelick et al*., 2005]. The temperature range over which the AFT system is most sensitive is 60–110°C, also called the partial annealing zone (PAZ), and for the AHe system it is 40–80°C, which is called the partial retention zone (PRZ) [*Gleadow et al*., 1986; *Farley*, 2002]. On the other hand, studies of basin subsidence provide important information about temporal variation of sediment flux into depocenters. Subsidence modeling relies on the back-stripping procedure especially adapted to terrestrial (nonmarine) basins [*Linol et al*., 2015c]. In this paper we compare the timing of erosion and deposition of the eroded part of the basement crustal rocks into an adjacent basin. We use both thermochronologic and subsidence data in order to quantify the amount and rates of unroofing of Tanzanian basement rocks which we compare to the subsidence of the adjacent Congo basin in the realm of central Gondwana.

We report AFT and AHe data from a ~ 2.2 km deep exploration borehole located in the Tanzanian Craton and surface samples from across the terrain extending westward to the Ubendian orogen, which is proximal to the western arm of the East African Rift System (EARS; Figure 2). Additionally, we use subsidence data from the Congo basin obtained from four boreholes drilled during the 1950s and 1970s (Figure 1 for locations). We also attempt to compare the magnitude of sediment yield to the volume of sediments deposited in the Congo basin.

2. Geological Setting

2.1. The Tanzanian Craton

The Archean bedrock of Tanzania comprises high-grade Dodoman Complex and the granite-greenstone sequences of the Nyanzian and Kavirondian Supergroups (Figure 2). These terrains exhibit diverse tectonic histories, including variable magmatism, sedimentation, and metamorphism [*Manya et al*., 2006; *Kabete et al*., 2012; *Kasanzu*, 2014]. The Dodoman Complex is composed of relatively high-grade facies orthogneisses, quartzites, and migmatites. *Kabete et al*. [2012] report a detrital zircon U-Pb date of 3.6 Ga from the

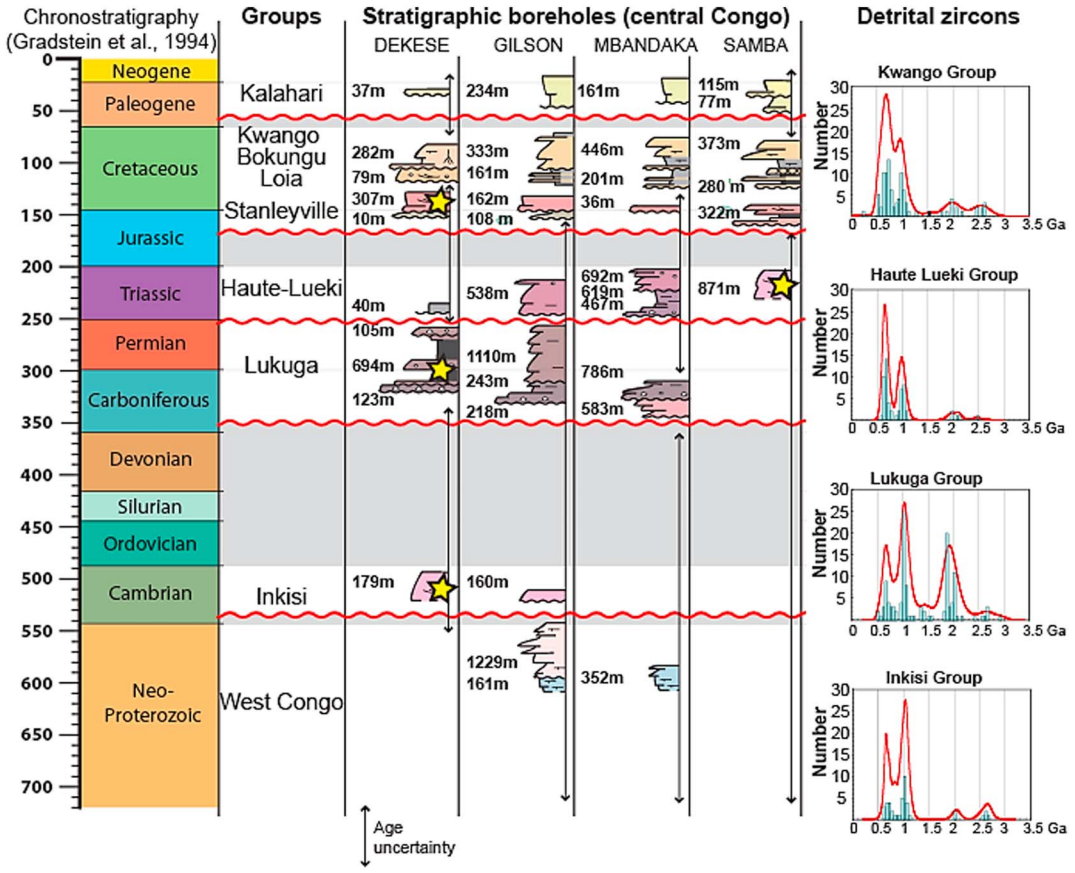

Figure 3. Stratigraphic details in the Congo basin showing the sampled sections (indicated as yellow stars). (right column) Detrital zircon U-Pb dates distribution frequency plots for stratigraphic units of basin. Grey colors indicate major hiatus. Red horizontal thick lines indicate major unconformities. Also note the Archaean signals obtained for Inkisi, Lukuga, Haute-Lueki, and Kwango Groups.

Dodoman terrain and interpreted it to be the basement rocks of the low-grade greenstone sequences of the Nyanzian and Kavirondian. Magmatic activity in the Nyanzian Supergroup is constrained by U-Pb dates ranging from 2.8 ± 0.3 Ga to 2.7 ± 0.9 Ga [*Borg and Krogh*, 1999; *Wirth et al.*, 2004; *Manya et al.*, 2006]. The Nyanzian and Kavirondian Supergroup rocks in the region are envisaged to be associated with subduction tectonism processes [*Manya et al.*, 2006]. Lithological assemblages include granitoids, basalts, pyroclastics, felsic flows, shales, mudrocks, and iron formations.

The craton is bounded by granulites of the Pan African Mozambique Belt to the east; the Eburnean Ubendian-Usagaran to the southeast, south, and southwest; the Kibaran Karagwe-Ankolean terrain to the northwest; and the Neoproterozoic clastic sedimentary sequences of the Malagarasi Supergroup [see *Deblond et al.*, 2001; *Tack et al.*, 2011]. However, no detrital U-Pb zircon data have ever been reported for these clastic sequences. Phanerozoic basins are present in the southern and eastern parts of the country (Figure 2). These basins are mainly Karoo sequences which reach a thickness of up to 3 km [*Wopfner*, 2002; *Linol et al.*, 2016]. The term Karoo in the region has been used to refer to late Carboniferous-Jurassic depositional sequences, which represent a regional erosional event that was associated with Gondwana tectonics [*Linol et al.*, 2016]. The rift flanks of the EARS form topographic highs along the western, northern, and northeastern margins of the craton (Figure 1 bottom) and the eastern branch of the rift have divided the cratonic margins since ~25–30 Ma [e.g., *Chorowicz*, 2005; *Wichura et al.*, 2015].

2.2. Congo Basin and Sediments Provenance

The Congo basin comprises 4–6 km of Neoproterozoic to Cenozoic sediment [*Linol*, 2013]. The upper Neoproterozoic to lower Paleozoic Inkisi redbeds are overlain by Carboniferous to Permian glacial sequences

AGU Tectonics

10.1002/2016TC004147

Table 1. Fission Track Results for Basement Rocks From Tanzania[a]

Sample ID	D./E. (m)	UTM	Litho.	Nc	ρs (N_s) ($\times 10^6$ cm^{-2})	ρi(N_i) ($\times 10^6$ cm^{-2})	U (μg/g) ± C.v.	$P(\chi^2)$ (%)	Var	Central Date (Ma) ± 1σ	CFTL (μm) ± 1σ	SD (μm)	Dpar (μm)	SD (μm)
TC02	−100	442425.5/9645439	Aggl.	20	0.46 (308)	0.37 (246)	3.3 (39)	94.4	0.0%	307.1 ± 32.6	12.6 ± 0.2 (45)	1.6	2.2	0.3
TC04	−200	442425.5/9645439	Andesite	11	0.56 (153)	0.45 (123)	3.9 (38)	99.2	0.0%	305.1 ± 43	-			
TC06	−300	442425.5/9645439	Andesite	20	0.78 (350)	0.64 (290)	5.8 (48)	99.9	0.0%	296.3 ± 31.8	12.4 ± 0.2 (31)	1.1	2.1	0.2
TC08	−400	442425.5/9645439	Aggl.	16	0.53 (234)	0.49 (203)	4.3 (35)	84.1	0.0%	281.4 ± 32.6	13 ± 0.4 (9)	1.3	2.3	0.1
TC12	−600	442425.5/9645439	Tuff	16	0.67 (210)	0.59 (184)	5 (41)	69.6	7.0%	275.4 ± 34.6	12.4 ± 0.5 (7)	1.2	2.2	0.2
TC14	−700	442425.5/9645439	Mudst.	20	0.49 (245)	0.44 (219)	4.1 (42)	97.5	0.0%	268.2 ± 31.6	12.3 ± 0.3 (13)	1.0	2.1	0.8
TC16	−800	442425.5/9645439	Tuff	20	0.66 (298)	0.60 (270)	5.3 (33)	1.9	32.0%	261 ± 34.5	13.7 ± 0.4 (3)	1.1	1.9	0.2
TC18	−900	442425.5/9645439	Aggl.	14	0.46 (156)	0.42 (143)	3.8 (62)	92.0	0.0%	265 ± 36.2	13.6 ± 0.1 (2)	0.2	2.2	0.2
TC22	−1100	442425.5/9645439	Aggl.	14	0.57 (173)	0.52 (157)	4.4 (60)	44.2	4.0%	267.9 ± 35.5	12.8 ± 0.6 (8)	1.3	2.8	0.6
TC26	−1300	442425.5/9645439	Aggl.	13	0.45 (148)	0.41 (135)	3.8 (40)	91.7	0.0%	264 ± 36.9	-			
TC30	−1500	442425.5/9645439	Andesite	20	0.35 (204)	0.33 (189)	3 (56)	96.0	0.0%	262 ± 32.6	12.1 ± 0.7 (7)	2.2	2.7	0.4
TC34	−1700	442425.5/9645439	Andesite	18	0.43 (237)	0.40 (221)	4 (80)	87.5	0.0%	260.6 ± 30.8	11.7 ± 0.4 (8)	0.7	2.1	0.3
TC40	−2000	442425.5/9645439	Andesite	7	0.35 (70)	0.35 (70)	2.9 (40)	87.8	0.0%	244.9 ± 45	10.8 ± 0.3 (23)	1.5	2.4	0.3
TC42	−2100	442425.5/9645439	Andesite	20	0.32 (175)	0.37 (201)	3.2 (45)	100.0	0.0%	215.1 ± 27.1	-	-	-	
TC44	−2200	442425.5/9645439	Andesite	6	0.32 (35)	0.43 (46)	3.6 (32)	95.7	0.0%	188.4 ± 44	-	-	-	
CK07	1198	484637/9527823	Granite	20	1.92 (832)	1.76 (760)	15.4 (57)	19.8	0.1%	261.3 ± 24.5	13 ± 0.5 (11)	1.3	2.7	0.2
CK08	1291	473162/9455056	Granite	20	0.58 (400)	0.44 (303)	3.7 (26)	100.0	0.9%	317 ± 33.3	12.1 ± 0.1 (32)	2.2	2.2	0.4
CK12	1167	282431/9440582	Granite	30	2.89 (876)	1.79 (798)	43.8 (26)	11.0	67.0%	275.7 ± 27.6	-	-	-	-
CK14	1151	233276/9437344	Gneiss	30	7.13 (2166)	6.90 (2100)	7.7 (62)	0.0	0.3%	266.2 ± 29.1	12.4 ± 0.2 (46)	1.3	3	0.8
CK15	997	210136/9436401	Gneiss	30	1.59 (763)	1.30 (627)	12.5 (51)	4.1	0.8%	285.1 ± 26.5	12.4 ± 0.2 (83)	1.1	3.5	0.5

[a]D= depth; E. = elevation; UTM = Universal Transverse Mercator; Litho. = lithology; Aggl. = agglomerate; Mudst. = mudstone; Nc = number of crystals dated; ρs = density of spontaneous tracks; ρi = density of induced tracks; Ns = number of spontaneous tracks; Ni = number of induced and dosimeter glass tracks; C.v. = covariance in %; $P(\chi^2)$ = chi-square probability; Var. = variation coefficient in %; CFTL = confined fission track length; SD = standard deviation.

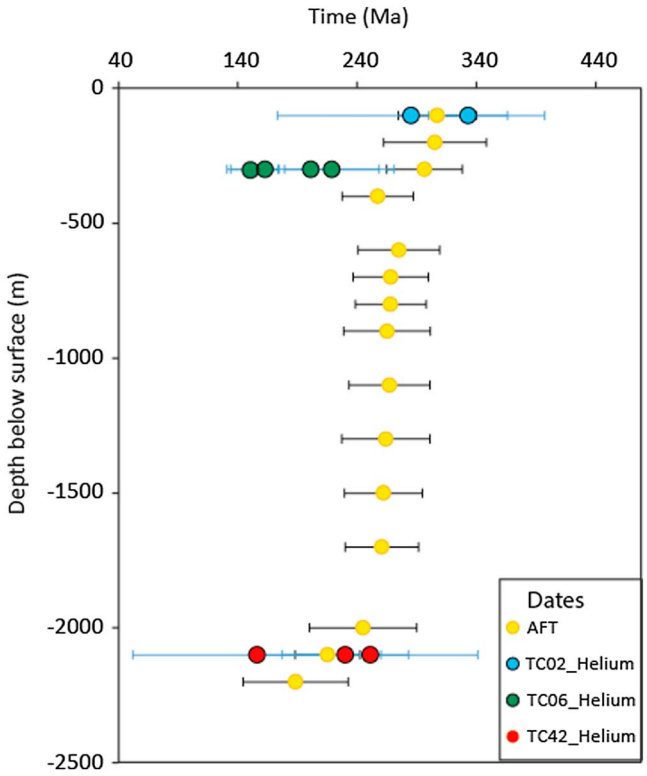

Figure 4. A plot displaying the single-grain, alpha-corrected apatite (U-Th)/He and central fission track dates with depth for the Bulyanhulu borehole samples.

of the Lukuga Group [*Bose and Kar*, 1978] (Figure 3), then Triassic Haute-Lueki Group, Upper Jurassic to Upper Cretaceous fluvial-lacustrine and aeolian sequences of red sandstones and mudstones of the Kwango Group, and Cenozoic alluvium deposits of the Kalahari Group. These sequences are separated by basin-wide unconformities (see Figure 3). The Lukuga, Haute-Lueki, and Kwango (only its basal unit) Groups constitute the equivalents of the Karoo sequences.

Detrital zircon dates for each stratigraphic unit are summarized in Figure 3. The redbeds of the Ikinsi Group have two dominant date populations of 1100–950 Ma and 800–600 Ma. These are most likely sourced from the Oubanguides of north central Africa [*Linol et al.*, 2015b]. Eburnian and Kibaran sources are dominant for the Lukuga Group, whereas the overlying Haute-Lueki Group detrital zircon data suggest a largely Pan African protolith (Figure 3). The uppermost Kwango Group, including the Stanleyville Formation, reveal four main date populations; 3.0–2.6 Ga, 2.1–1.8 Ga, 1 Ga, and 0.85–0.5 Ga (Figure 3) [*Linol et al.*, 2015b] that suggest mixed Precambrian sources. Paleocurrents were from the east, implying that the Tanzania Craton was one of the source terrains that supplied detritus to the basin [e.g., *Linol*, 2013].

3. Analytical Methods: AFT and AHe Thermochronometry

Fifteen subsurface samples collected from the Bulyanhulu borehole (surface elevation is 1184 m) (Figure 2) were dated using the external detector method for AFT; confined fission tracks lengths were measured, and the etch pit diameters (i.e., kinetic parameter, Dpar) values were also measured for each sample. Sampled lithologies from the borehole include granites, andesites, mudstones, tuffs, and agglomerates. Surface cratonic granite samples (CK07, CK08, and CK12) together with two Ubendian gneissic samples (proximal to the rift; CK14 and CK15) were also included in the analyses.

Mineral separation and sample preparation was conducted at the University of Glasgow. Mounts of apatite grains were etched using a 5 M HNO_3 solution at 20°C for 20 s to expose spontaneous tracks from ^{238}U. Three IRRM glass monitors with U content of 10 ppm each were used for irradiation. These samples were irradiated with thermal neutrons at the nuclear reactor at Oregon State University (USA). Following irradiation, the mica detector samples were etched using 40% HF acid at 20°C for 36 min to reveal induced tracks from ^{235}U. Counting of tracks was performed using a 1250X magnification Zeiss Axiotron microscope and computer-controlled *x-y* stage system (FTStage). Date computations were accomplished using a zeta calibration factor of 320 ± 21 for C.H. Kasanzu and the software TrackKey version 4.2 by *Dunkl* [2002].

Individual apatite grains were screened based on their clarity and morphology and handpicked for (U-Th)/He analysis then packed into Pt tubes prior to analysis. Helium, U, and Th analyses were performed at the Scottish Universities Environmental Research Centre (SUERC). The analytical protocol adopted in this study follows that described by *Foeken et al.* [2006, 2007]. Length and width measurements for alpha ejection correction (Ft) [*Farley*, 2002] were taken for each grain. (U-Th)/He dates were calculated using standard

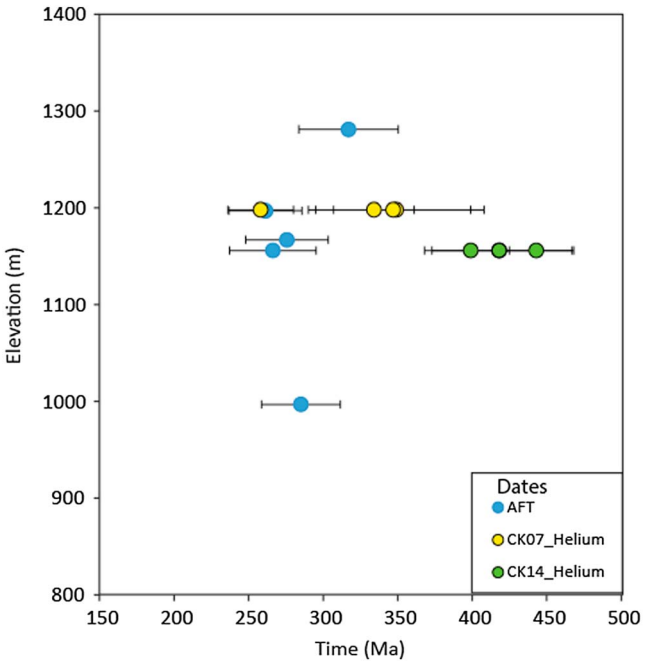

Figure 5. Central apatite fission track and single-grain, recoil-corrected (U-Th)/He dates versus elevation for surface samples from Tanzanian basement rocks.

procedures developed by *Meesters and Dunai* [2002]. Total analytical uncertainty was computed as a square root of squares of weighted uncertainties of U, Th, and He measurements and including the estimated additional variation of ±7% determined on repeat analyses of Durango apatite.

4. Results

4.1. AFT Data

AFT data are presented in Table 1 and are graphically displayed in Figures 4 and 5. Basement samples collected from the Bulyanhulu borehole reveal a tight cluster of Permian-Triassic (296 ± 32 to 215 ± 27 Ma) except for samples TC02, TC04, and TC44 that yielded Carboniferous dates of 307 ± 33 Ma and 305 ± 43 Ma and Jurassic dates of 188 ± 44 Ma, respectively. AFT dates from outcrop samples range between 317 ± 33 and 261 ± 25 Ma (Upper Carboniferous to Upper Permian, respectively). Mean track lengths for all samples vary between 13.7 ± 0.4 and 10.8 ± 0.3 μm, with a standard deviation of 0.8 μm, and Dpar range between 1.9 and 3.5 μm, with a standard deviation of ~ 0.3 μm. The number of confined track lengths was lower in our samples due to low uranium contents and thus low track density. None of the samples used in this study were from within the PAZ (based on mean surface temperature of 25°C and current gradient of 9°C/km which is obtained from the model results) where enhanced annealing of apatite fission tracks takes place. The deepest samples were sampled from 45–55°C and so may have experienced some track annealing. The dates are also much younger than the stratigraphic ages (Archean-Proterozoic), implying that all samples have experienced significant thermal annealing and subsequent Phanerozoic cooling below the 110°C isotherm. All samples pass the chi-square test except for TC16, CK14, and CK15.

4.2. (U-Th)/He Data

Apatite (U-Th)/He dates were determined on 16 single grains from three borehole samples (TC02, TC06, and TC44) and two outcrop samples (CK07 and CK14). The samples yielded α-ejection corrected single-grain dates ranging between 333 ± 33 Ma and 285 ± 112 Ma (Table 2 and Figure 4; for shallowest sample at 100 m below surface) and between 251 ± 90 Ma and 156 ± 104 Ma (for deepest sample at 2100 m below surface). In contrast, surface samples CK07 and CK14 yielded (U-Th)/He dates ranging between 349 ± 59 and 258 ± 22 Ma and between 399 ± 26 to 443 ± 24 Ma, respectively (see Figure 5), which are somewhat older than the corresponding AFT dates. All helium dates are single-grain dates, and errors are 1 sigma. All samples (except for sample TC42; −2100 m; ~40°C) do not currently reside in the AHe PRZ. This indicates that AHe dates, which are all significantly younger than the Precambrian emplacement ages for these rocks, reflect elevated paleotemperatures followed by subsequent cooling to below 80°C during or after the Paleozoic.

Grains TC02#06, TC42#01, and TC42#02 and most of the CK07 and CK14 aliquots yielded (U-Th)/He dates that are significantly older than corresponding central AFT dates in this study (Figures 4 and 5). Similar observations of older AHe dates relative to their corresponding apatite fission track dates have been reported in a number of other studies of cratonic regions [e.g., *Lorencak*, 2003; *Belton et al*., 2004; *Green et al*., 2006; *Flowers and Kelley*, 2011]. This can be explained by the low effective helium diffusivity in grains with high radiation damage. Other additional causes of dispersion of grain dates may include helium implantation

Table 2. Apatite (U-Th)/He Data for Basement Samples [a]

Sample #Grain	D./E. (m)	UTM	Nc	L (μm)	W (μm)	T	Th (ppm)	U (ppm)	eU (ppm)	4He (cc as STP)	Unc. Date (Ma)	Ft	Cor. Date (Ma)	Error (Ma)
TC02#12	−100	442425.5/9645439	1	145	100	2	5	2	3	1.77E−12	208	0.73	285	112
TC02#06	−100	442425.5/9645439	1	190	172	1	31	3	10	1.55E−09	276	0.83	333	33
TC06#04	−300	442425.5/9645439	1	145	60	1	42	4	14	1.91E−10	120.2	0.61	201	70.1
TC06#03	−300	442425.5/9645439	1	134	98	1	54	3	15	6.11E−10	111.1	0.72	154.3	20.2
T0C6#02	−300	442425.5/9645439	1	190	75	0	28	3	9	3.65E−10	148.8	0.68	218.7	39.6
TC06#10	−300	442425.5/9645439	1	164	105	0	30	4	11	6.48E−10	121.7	0.75	162.6	11.1
TC42#01	−2100	442425.5/9645439	1	64	66	1	75	20	38	4.30E−11	129	0.52	251	90
TC42#02	−2100	442425.5/9645439	1	98	56	1	323	27	102	2.59E−11	122	0.53	230	53
TC42#18	−2100	442425.5/9645439	1	120	75	1	11	3	5	1.29E−10	101	0.65	156	104
CK07-3	1198	484637/9527823	1	132	55	1	35	18	26	5.1 + E−10	196	0.56	349	59
CK07-6	1198	484637/9527823	1	129	90	1	29	15	22	2.00E−09	180	0.7	258	22
CK07-2	1198	484637/9527823	1	111	81	1	20	15	19	8.59E−10	230	0.66	347	52
CK07-7	1198	484637/9527823	1	209	107	1	14	7	11	1.96E−09	259	0.77	334	27
CK14-2	1156	233276/9437344	1	258	81	1	24	102	108	1.61E−08	285	0.71	399	26
CK14-3	1156	233276/9437344	1	220	95	1	38	82	91	2.13E−08	330	0.74	443	24
CK14-4	1156	233276/9437344	1	135	107	1	11	88	91	1.35E−08	309	0.74	418	50

[a]All data are calculated following the formula in *Meesters and Dunai* [2002].
L = length; W = width; T = terminations; eU = effective uranium calculated as [U] + 0.235*[Th] [*Flowers et al*., 2009]; Unc. = uncorrected; Ft = correction factor; Cor. = corrected. Other abbreviations as in Table 1.

[*Spiegel et al*., 2009], uranium-bearing mineral and/or fluid inclusions, and effects of uranium-bearing coatings on grains or grain boundaries [e.g., *Murray et al*., 2014].

In our study, no samples display clear correlations between grain dates and grain sizes (i.e., radii; Figures 6c and 6d). This may in part reflect the small to moderate range of grain size (40–70 μm). In Figure 6a the relationship between AHe dates versus effective uranium (eU) is shown for the Bulyanhulu samples. Only sample TC42 shows signs of a positive correlation between date and eU, and sample TC02 shows a weaker correlation (based on only two grains). The limited number of dated grains for these two samples though makes it difficult to evaluate the significance of these correlations. The eU range for sample TC06 is small, and so the eU effect is not expressed strongly by this sample. The eU content for sample CK07 is high (40–100 ppm). The effect of eU is often saturated at these levels, explaining why the correlation between grain dates and eU is not clear (Figures 6 and 6db). *Brown et al*. [2013] demonstrated that the competing effects of grain size, eU, and fragmentation act to disrupt the simple correlations expected between grain size, eU, and grain dates and so this sort of behavior, as shown in Figure 6, is to be expected for samples with complex histories and significant helium loss.

Fission track density distributions are homogeneous, which tends to rule out U and Th zoning as explanation for the date dispersion. However, the relatively low eU values for these grains (except for TC42) make them susceptible to the influence of helium implantation from outside the grain and thus the spread in dates. Overall, though, we believe the AHe date dispersion observed is consistent with the combined effects of eU and grain size variation and the fact that the samples have experienced prolonged residence within the partial helium retention zone.

5. Thermal History Modeling

Optimum thermal history models were determined using the inverse approach explained in detail by *Gallagher* [2012] and

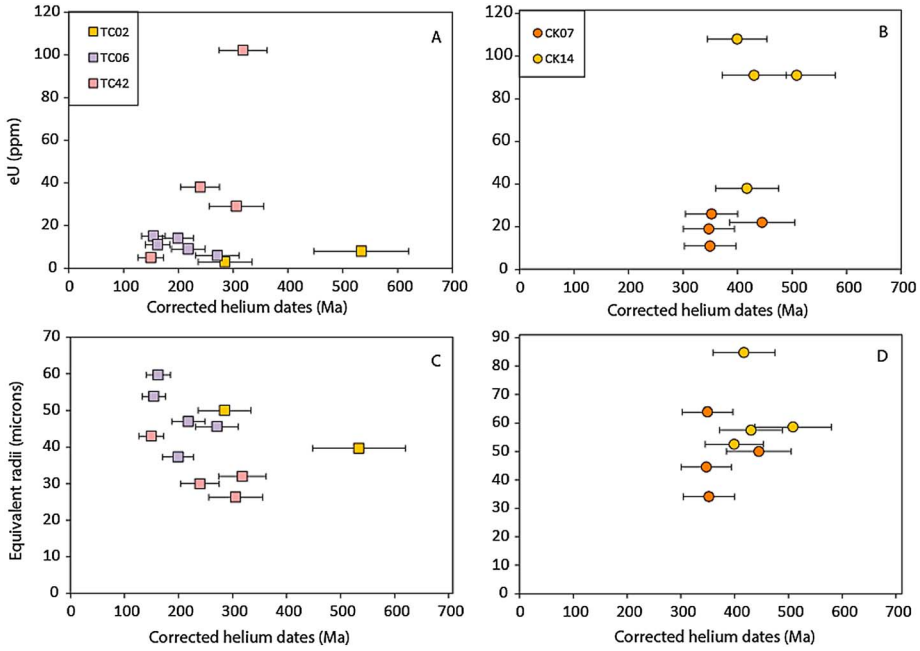

Figure 6. Binary plots showing the relationship between effective uranium and alpha-corrected (U-Th)/He dates for (a) borehole and (b) surface samples; the relationship between corrected helium dates against corresponding equivalent radii for (c) borehole and (d) surface samples.

jointly modeling AFT and AHe data using the QTQt software where both AFT and AHe were available. To account for the effects of radiation damage accumulation and annealing on the diffusivity of helium in apatite, we use the radiation damage model of *Gautheron et al*. [2009]. Due to the lack of robust geological constraints on the thermal histories, the initial model constraints allowed samples to pass between 0°C and 140°C any time between 600 Ma and 400 Ma (before the oldest fission track date of 307 ± 33 Ma). Joint inverse modeling of multiple samples from different depths enables an independent estimate of the paleogeothermal gradient. Modeling results indicate that Paleozoic to recent paleogeothermal gradients for the studied sites were similar to the present day (nominal geothermal gradient of ~9°C/km for craton and 25°C/km for the Ubendian samples). This observation is important in this context, as it indicates that the Paleozoic cooling recorded by the AFT and AHe data must have occurred because of erosion of crustal material and cannot be explained by cooling caused by a transient increase in the geothermal gradient.

5.1. Bulyanhulu Borehole Model

The optimum expected model for the Bulyanhulu borehole data is shown in Figure 7a, and a comparison between the observed and predicted data is provided in Figure 7b. The model indicates protracted cooling over 140 Ma of the cratonic samples through the PAZ and PRZ starting in the Carboniferous (340 ± 30 Ma) followed by residence at or near-surface temperatures of ~20–30°C since ~200 Ma.

5.2. Outcrop Sample Models

The optimum expected model for surface cratonic samples CK07, CK08, and CK12 is shown in Figure 8a, and a comparison between observed and predicted data is shown in Figure 8b. The data for these samples were jointly modeled as a coherent sequence because all three samples are from cratonic basement and are not separated by any major structures. The thermal history for these samples also indicates strong Carboniferous cooling starting at 340 ± 30 Ma as seen for the Bulyanhulu data. The model suggests that these samples cooled from maximum paleotemperatures of 90 ± 30°C to 40 ± 12°C by ~280 Ma. This early maximum temperature is slightly lower than the near-surface samples from Bulyanhulu, but the uncertainty on the maximum temperature is large, and so these samples may have cooled from maximum paleotemperatures similar to the Bulyanhulu (i.e., 110–120°C). This cooling was followed by a protracted period of stability through to the early mid-Cretaceous when cooling resumed, but at much lower rates, and the samples finally reached present surface temperatures of 20–30°C.

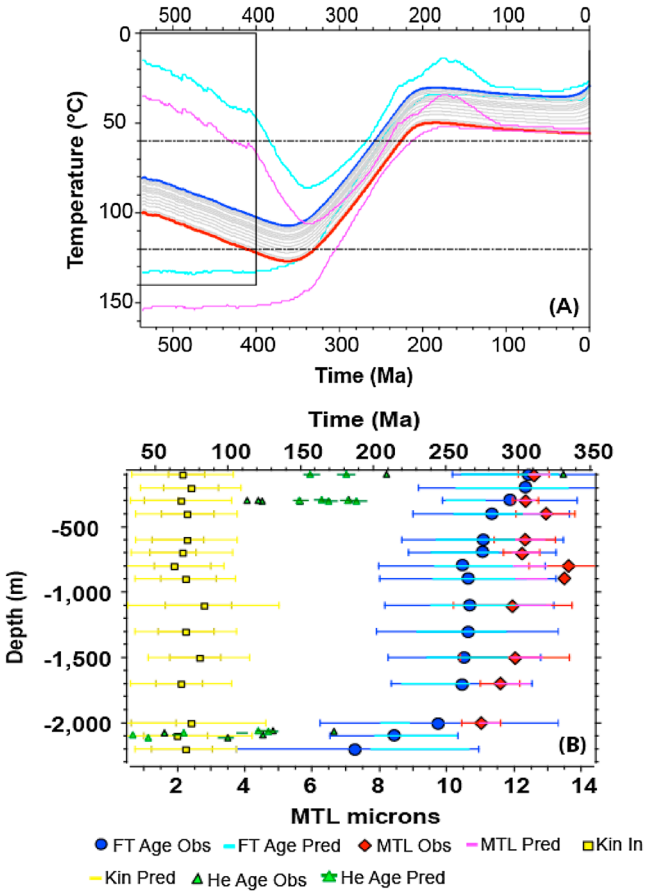

Figure 7. *T-t* cooling histories of all borehole samples modeled using both AFT and (U-Th)/He data using the approach described by *Gallagher* [2012] and performed using QTQt software. In this model, the radiation damage approach by *Gautheron et al*. [2009] was used. (a) *T-t* cooling histories of all borehole samples modeled using both AFT and helium data. The solid dark blue line represents the thermal history for the shallowest sample in the profile (TC02), and the solid red line represents the thermal history for the deepest sample in the profile (TC44). The thinner purple/pink lines are the 95% confidence interval for the deepest sample history, and the thinner light blue lines are the 95% confidence interval for the shallow sample history. (b) Summary of the predicted and observed data.

Samples CK14 and CK15 were modeled using the same approach; the optimum expected thermal history model is shown in Figure 9a, and a comparison between observed and predicted data is shown in Figure 9b. The two samples were both collected within the Ubendian orogen and adjacent to the western rift and are treated as a coherent vertical profile. Like previous models from the craton interior, significant Carboniferous (340–290 Ma) cooling (70 ± 25°C) is indicated (Figure 9a). However, in contrast to the craton samples, the model suggests that these samples experienced significant additional cooling of 30 ± 15°C starting in the mid-late Cretaceous (80–60 Ma). Although this later episode is not well resolved by our current data from the craton, it is consistent with conclusions from several other thermochronology studies in East Africa [*Foster and Gleadow*, 1992, 1996; *Noble et al*., 1997; *Mbede et al*., 1993; *Spiegel et al*., 2007].

The period of Carboniferous cooling is consistently recorded by all samples. Subsequent to this early cooling episode, the cratonic samples from Bulyanhulu and the outcrop samples CK07, CK08, and CK012 experienced relative stability and/or only minor additional cooling (30°C) through to the present. In contrast, the modeling results suggest that the two samples, CK14 and CK15, experienced a later cooling initiated between 80 and 60 Ma. Although the magnitude and timing of this later phase is not well constrained by our data, it is significant that previous thermochronological studies focused on the EARS and rift margins in Tanzania [*Noble et al*., 1997; *van der Beek et al*., 1998] and farther north in Kenya [*Foster and Gleadow*, 1992, 1996; *Spiegel et al*., 2007; *Torres-Acosta et al*., 2015] all document significant mid-late Cretaceous cooling of exposed basement rocks.

6. Subsidence Data Model for the Congo Basin

Subsidence of the Congo basin is analyzed by back-stripping the stratigraphic records of the four existing deep boreholes (approximately between 2 km and 4 km in depth) drilled near the center of the basin (see Figure 3 for borehole sequence thicknesses) [*Linol*, 2013]. The back-stripping procedure removes the effect of sediment loading from the basement subsidence, thus allowing quantification of the tectonic subsidence [e.g., *Allen and Allen*, 2005]. This is performed by correcting for sediment compaction at the respective depths and times of deposition of each stratigraphic unit, using empirical porosity/depth parameters linked to the proportion of clay and silt compared to sand of each stratigraphic unit, determined during logging of the boreholes.

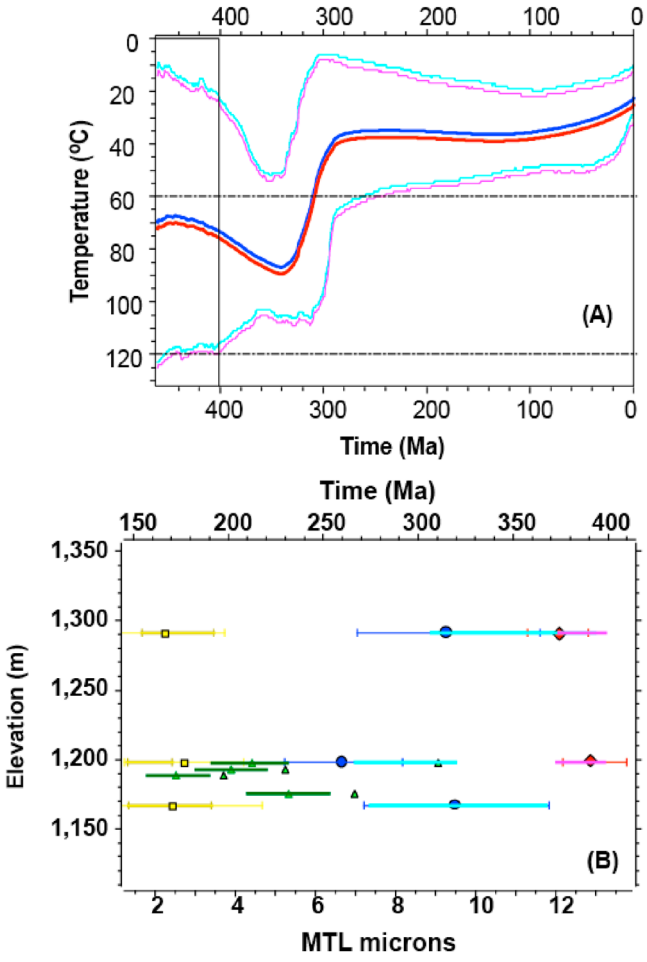

Figure 8. QTQt inverse thermal history modeling results using the approach described by *Gallagher* [2012] for data from samples CK07, CK08, and CK12. In this model the radiation damage approach by *Gautheron et al.* [2009] was used. (a) *T-t* cooling histories of the samples modeled. (b) Summary of the predicted and observed data. Other abbreviations of terms as in Figure 7.

The subsidence curves show the existence two main episodes of rapid subsidence. The first and most pronounced episode of subsidence (mean rate = 10–20 m/Ma; Figure 10) starts at 350 Ma with the onset of the main Gondwana (Carboniferous) glaciation and terminates at about 180 Ma as recorded at Mbadaka, Gilson, and Dekese (Figure 10). This corresponds to deposition of the Lukuga and Haute-Lueki Groups in the basin. The latter is attenuated to a thickness of only 40 m in the Dekese section, suggesting an episode of erosion during the Triassic.

A second main episode of subsidence (mean rate = 5–10 m/Ma; Figure 10) is apparent in all boreholes. It started at 160 Ma and lasted until 34 Ma. This corresponds to the deposition of the Stanleyville, Loia, Bokungu, and Kwango Groups. This history reveals two distinct phases of rapid subsidence: the late Jurassic, 160 Ma to 140 Ma, and the late Cretaceous to earliest Paleogene from 100 Ma to 34 Ma, in the four boreholes [*Linol et al.*, 2015c].

7. Discussion

7.1. Tectonothermal Implications of the Thermochronological Data

Thermochronology documents a major period of accelerated cooling, interpreted here as exhumation (uplift and erosion), beginning in the early mid-Carboniferous (between 340 and 280 Ma). A summary of the estimated cooling and the inferred amount and rate of erosion implied by the thermal history modeling is presented in Table 3. Within the craton interior the episode of early Carboniferous-Triassic cooling appears to have been prolonged over periods of 50 to 140 Ma, ending at 200 ± 20 Ma. These rocks then remained at or very near the surface until the present day.

Basement rocks from the craton were within the uppermost 10 km of the crust by the mid-Paleozoic and were exhumed at moderate rates (56–96 m/Ma) to within 1–2 km of the surface by the early Triassic. For the Bulyanhulu site specifically, *Nyblade* [1997] determined a thermal gradient of 8.7 ± 2.6°C/km (2sigma) from the borehole. This is within error of the paleogeothermal gradient of 9°C/km estimated by the *T-t* modeling of the Bulyanhulu borehole data (Table 3). Using this average geothermal gradient for the craton, 8.9 ± 2.4 km of crust has been removed at an average denudation rate on the order of 56 ± 21 m/Ma. Likewise, the Ubendian orogenic samples (CK14, CK15), with a geothermal gradient of 25°C/km, requires exhumation of 4.0 ± 1.7 km of crust since the Carboniferous (Table 3).

The Carboniferous-Triassic exhumation might be linked to the end Paleozoic far-field regional compressional tectonics during the formation of the Mauritanian-Variscan Orogeny when Pangaea assembled at 325–275 Ma, when Tanzania was at the heartland of Gondwana, and followed directly by the Gondwanide orogeny and formation of the Cape-de la Ventana fold and thrust belt between 276 and 248 Ma [*Linol*

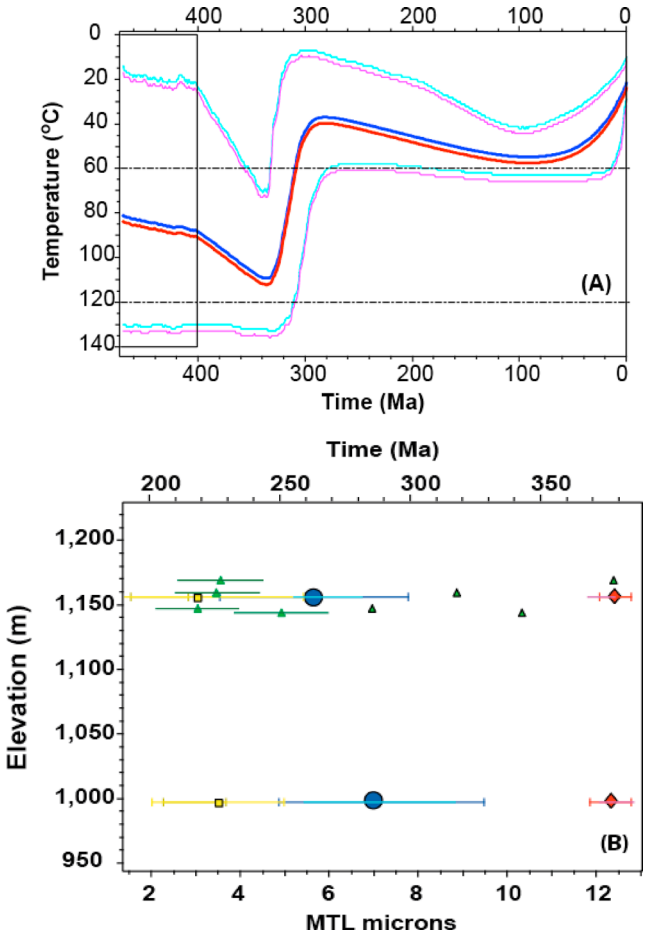

Figure 9. QTQt inverse thermal history modeling results using the approach described by *Gallagher* [2012] for data from samples CK14 and CK15. (a) *T-t* cooling histories of the modeled samples. (b) Summary of the predicted and observed data. The estimated paleogeothermal gradient for this model was approximately 25°C/km. Other symbols as in Figure 7.

et al., 2015c, and references there in]. It is thus possible that the first commencement of exhumation in Tanzania may have been triggered by far-field intraplate stresses between 350 and 250 Ma. The timing of this phase of enhanced erosion between 340 and 280 Ma also overlaps with estimates of the period of major glaciation across Gondwana [*Isbell et al.*, 2003], and so it is also possible that erosion rates were partly enhanced by glacial processes.

The later phase of exhumation most clearly detected by the samples closest to the western rift (CK14 and CK15) commenced at 70 ± 20 Ma and resulted in the removal of 1.2 ± 0.6 km of crust at a mean rate of 17 ± 10 m/Ma (Table 3). Notwithstanding the poor resolution of this later phase of cooling by our data, the modeling results indicate similar amounts (less than 1.3 km) at somewhat lower rates (between 5 and 12 m/Ma) of erosion since 200 Ma for the interior cratonic regions (Table 3). Paleogene exhumation has been reported in other studies in the region and in East Africa [e.g., *Foster and Gleadow*, 1992, 1996; *Noble et al.*, 1997; *Mbede et al.*, 1993; *Bauer et al.*, 2010; *Torres-Acosta et al.*, 2015]. The available published AFT data are summarized in Figure 11. The pattern of AFT dates clearly shows that the younger AFT dates (less than 100 Ma) occur predominantly along the rifted craton margin and within the rifts of the EARS, while the oldest dates occur within the craton interior. This spatial pattern of AFT dates across Tanzania provides an excellent proxy for the timing of major erosion and highlights that the younger phases of erosion are focused along the craton margins and rift flanks of the EARS.

This late Cretaceous-early Tertiary exhumation significantly postdates the formation of the African plate during the start of the opening of the Indian (160 Ma) and South Atlantic (134 Ma) Oceans. However, this exhumation period partly overlaps in time with local kimberlitic emplacements which took place between 60 and 34 Ma within the craton (H. A. Jelsma, personal communication, 2013). This observation may suggest some degree of geodynamic interactions between the deep-seated mantle material and the cratonic lithosphere causing surface uplift by up-doming of the region [e.g., *Torres-Acosta et al.*, 2015]. Because tectonomagmatic activities (e.g., kimberlite emplacement) documented in southern Africa and their role in triggering exhumation has been linked to the African Superswell, the exhumation during the Paleogene in Tanzania may also be associated with deep-seated mantle processes [*Tinker et al.*, 2008; *Wichura et al.*, 2015; *French and Romanowicz*, 2015; *Torres-Acosta et al.*, 2015; *Koptev et al.*, 2015].

7.2. Linking Exhumation and Subsidence

Evidence of significant exhumation and erosion across the heartland of Gondwana has been increasingly revealed through thermochronologic studies in eastern Central Africa [*Foster and Gleadow*, 1992, 1996;

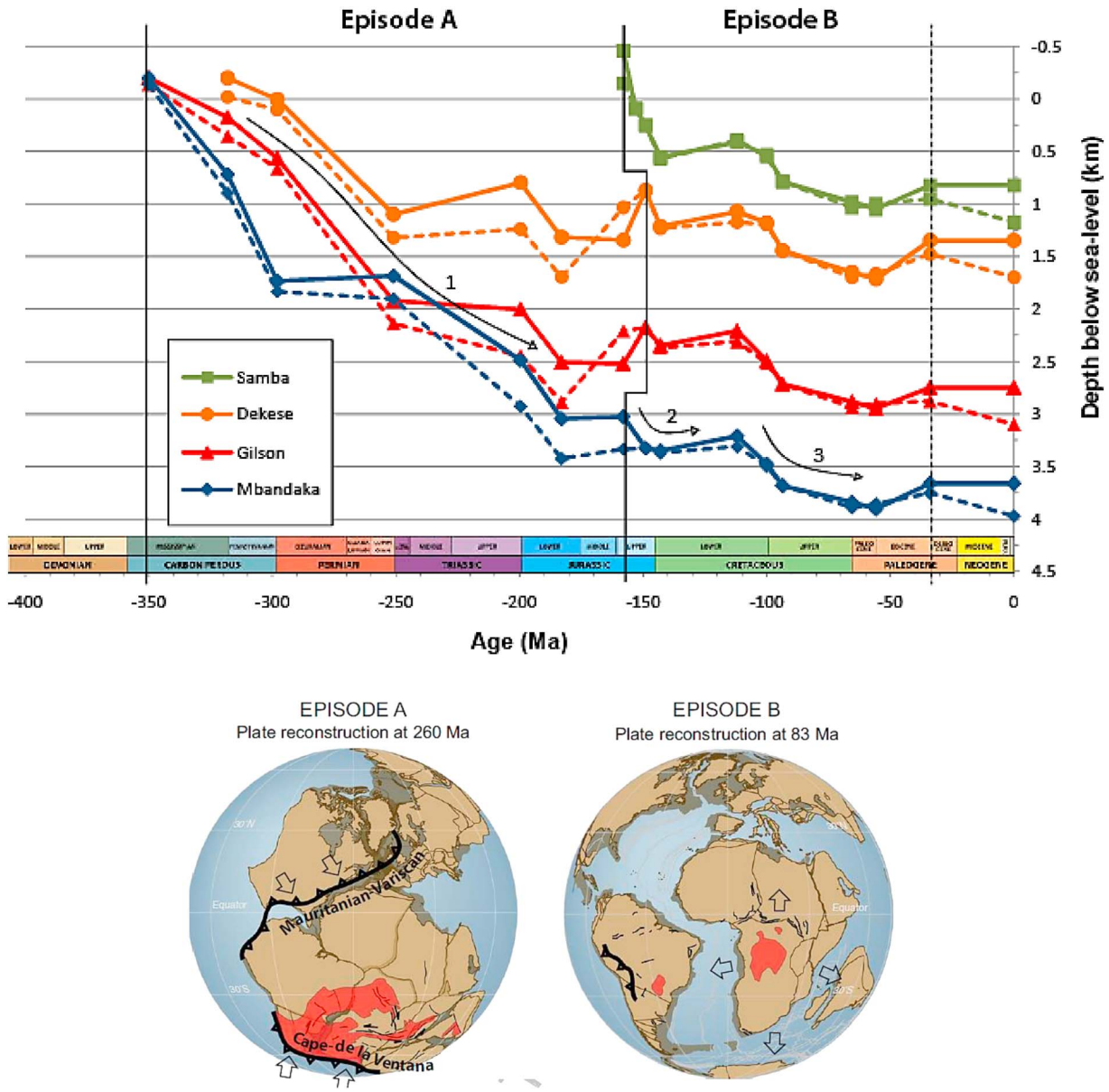

Figure 10. (top) Tectonic subsidence curves for the Congo basin. The curves show two main episodes of subsidence (A and B), including three phases of rapid subsidence (1–3, arrowed) separated by episodes of slower subsidence. Hashed lines correspond to calculated subsidence without paleotopography input (paleoelevation = 0). (bottom left) Plate reconstruction showing dominant compressional tectonics within Pangea that coincides with Episode A in the basin; (bottom right) prevalent extensional tectonics within Africa related to mantle upwelling and seafloor spreading, overlapping with Episode B in the basin (red). Red in A = Karoo-Parana basin; in B Africa red = Congo basin (adopted from *Linol et al.* [2015c]).

Noble et al., 1997; *Mbede et al.*, 1993; *Spiegel et al.*, 2007; *Kasanzu*, 2014]. The record of sedimentation within adjacent basins might be expected to reflect the erosion of the basement rocks of these regions, including Tanzania. Deposition during these times took place between late Carboniferous and Triassic in the southern Tanzania Phanerozoic basins and possibly earlier (Visean-Namurian, 347–333 Ma) in the Congo basin [*Kadima et al.*, 2011; *Linol et al.*, 2015c].

AFT and AHe data reveal crustal erosion rates across the Tanzania Craton of 56 ± 21 m/Ma (Figures 7a and 8a) between 340 and 200 Ma. Evidence of accelerated subsidence (10–20 m/Ma; Figures 10 and 12) in the Congo basin during that time may indicate sediment influx, linking to erosion of surrounding hinterlands including the Tanzanian basement rocks. Detritus from Archean sources similar to dates of basement rocks of the craton is supported by detrital zircon dates reported in *Linol et al.* [2015b]. The weak zircon U-Pb Archean

Table 3. Erosion Estimates Derived From Thermal Model Results[a]

	Cooling From *T-t* Modeling				Estimated Erosion					
Samples	Onset (Ma)	End (Ma)	Duration (Ma)	Uncertainty (Ma)	Cooling (°C)	Uncertainty (°C)	Amount (km)	± Error (km)	Rate (m/Ma)	± Error (m/Ma)
CK15 and CK14							**25 ± 5°C/km**		**25 ± 5°C/km**	
Early phase	340	290	50	30	70	25	2.8	1.1	56	41
Late phase	70	0	70	20	30	15	1.2	0.6	17	10
CK12, CK07, and CK08							**9 ± 2°C/km**		**9 ± 2°C/km**	
Early Phase	340	280	60	30	52	30	5.8	3.5	96	76
Late Phase	110	0	110	40	12	5	1.3	0.6	12	7
Bulyanhulu borehole							**9 ± 2°C/km**		**9 ± 2°C/km**	
Early Phase	340	200	140	40	80	15	8.9	2.4	63	25
Late Phase	200	0	200		poorly resolved		<1?		~ 5–10?	

[a]Time of onset, duration, amount of cooling, and an indication of the uncertainty for each group of samples was extracted from the thermal history models discussed in the text. The erosion amounts and erosion rates are calculated using the thermal gradient (with nominal errors), and the errors on the amount of erosion and erosion rates were estimated by propagating the uncertainties on all estimates (added in quadrature). The geothermal gradients are in bold.

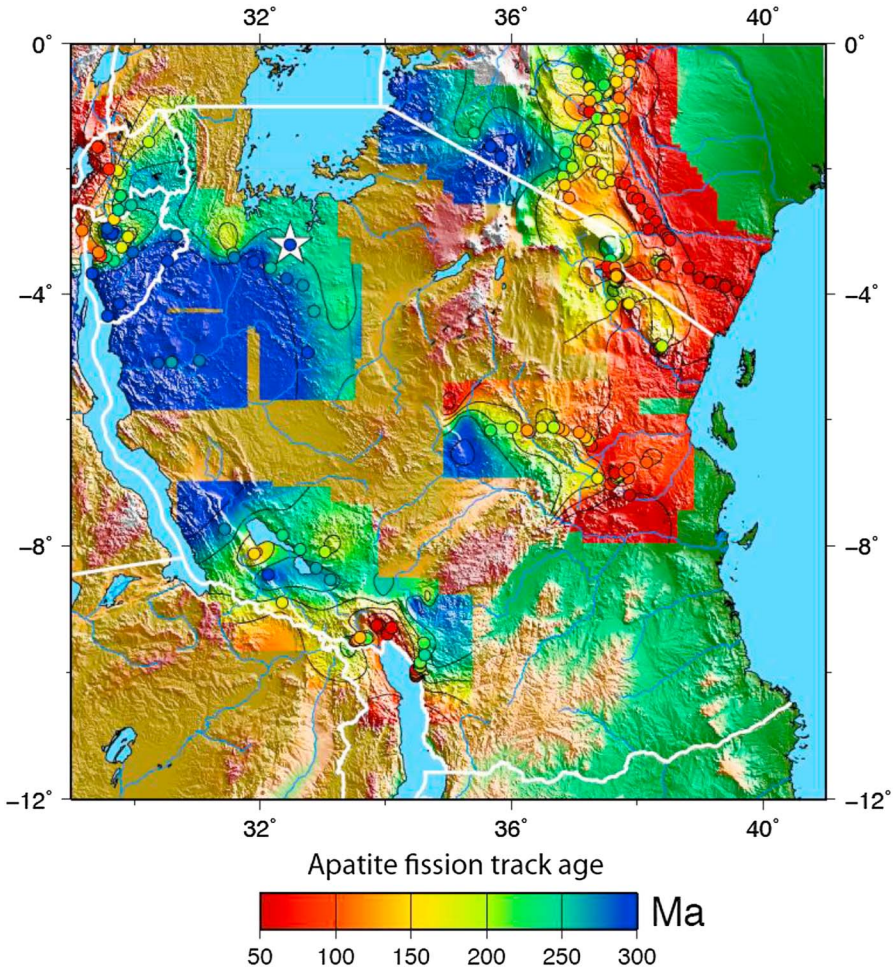

Figure 11. Map illustrating the regional pattern of AFT dates of surface rocks across the Tanzanian Craton and adjacent rifts of the EARS. Data are from *van den Haute* [1984], *Foster and Gleadow* [1992, 1993, 1996], *van der Beek et al.* [1998], and this study. The location of the Bulyanhulu borehole is indicated by the white star.

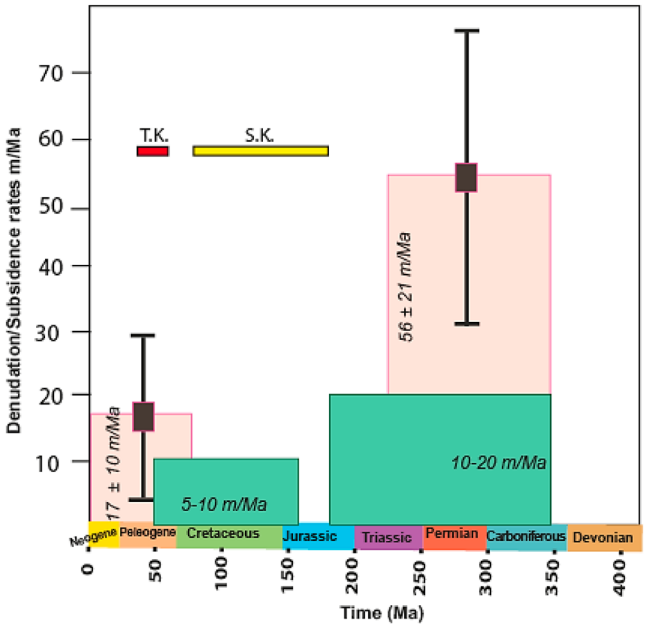

Figure 12. Denudation (pink) and subsidence (green) rates between the Tanzanian basement rocks and the Congo basin, respectively. TK and SK stand for Tanzania and South Africa kimberlite emplacements, respectively.

signal in the Congo basin may indicate that during that time, the Tanzania Craton was likely covered by late Neoproterozoic to Cambrian foreland basin sedimentary rocks, which were then part of the removed cover, consistent with the detrital zircon dates of Eburnian-Kibaran. In addition, recent stratigraphic analyses of the Karoo sedimentary sequences of Congo basin suggest a large easterly influx of sediments during the Carboniferous-Triassic and prior to Cretaceous [*Linol et al.*, 2015b]. A total sediment thickness of about 3.5 km was deposited in the basin between 350 and 250 Ma during the time of extensive early exhumation of the Tanzanian Craton [*Linol*, 2013]. This cycle of exhumation-subsidence is roughly contemporaneous across central, southern, and eastern Africa and also overlaps in time with the Mauritanian-Variscan collision and the formation of the Sierra de la Ventana-Cape Fold Belts (Figure 10) [*Linol et al.*, 2015c; *Kasanzu*, 2014]. The contemporaneous exhumation-subsidence events in the two regions (Figure 12) may indicate regional flexural readjustment of the lithosphere due to lithosphere buckling induced by far-field compressional tectonic processes, followed by deep mantle upwelling and epeirogenic processes. The change from rapid exhumation to slow cooling in the Tanzanian Craton at 200 ± 20 Ma overlaps with reduced sedimentation in the Congo basin between 180 and 160 Ma, as evidenced by a large hiatus [*Linol et al.*, 2015c].

The exhumation of the Tanzanian Craton during the Paleogene (~70 Ma onward; rates = 5–17 m/Ma; Figures 7 and 8) indicated by the surface and borehole samples postdates the onset of major subsidence in the basin during the Cretaceous (Figures 10 and 12). The amount of erosion ranges from 1.2 ± 0.6 km along the western craton margin to 1.3 ± 0.6 km of denudation within the interior of the craton at rates between 5 and 17 m/Ma. These reduced erosion rates and presumably reduced sediment flux from the craton coincides with a distinct but moderate (400–500 m) phase of uplift of the Congo basin that began at ~60 Ma (Figure 10).

8. Conclusions

Analysis of model thermal histories constrained using combined AFT and AHe thermochronometry data from the Tanzania Craton and sedimentation and subsidence histories of the Congo basin indicates that the emergence and exhumation of the craton and sediment accumulation and subsidence of the basin in central Gondwana, and later Africa, operated in tandem.

The study has documented an important Phanerozoic tectonic uplift/exhumation phase affecting basement rocks of Tanzania during the Carboniferous-Triassic (340–220 Ma; rate = 56–96 m/Ma). The cratonic interior subsequently remained stable with the current exposed rocks at or near (≤~1 km) the surface from ~200 Ma until final exhumation through the Cretaceous and Tertiary at much reduced rates of ~17 m/Ma. The onset of exhumation during the Carboniferous is coeval with major subsidence of the Congo basin, and we suggest that it is most likely induced by far-field stress due to compressional tectonics during Pangaea assembly (325–275 Ma) and the Gondwana Orogeny (276–248 Ma).

In contrast, the post-Jurassic history of the cratonic interior is characterized by relative stability and much reduced erosion (Table 3). The regional pattern of uplift and erosion across the craton and extending into the rifts to the east and west includes discrete phases of younger uplift and erosion during the early

Cretaceous and late Cretaceous-early Tertiary, which primarily effected the margins of the craton and the uplifted rift flanks (Figure 11) and which are also partly contemporaneous with subsidence in the basin. These younger events have been ascribed to a combination of African plate reorganization and the formation of the EARS, which has been linked with deeper mantle dynamics that dictated the evolution of the African Superswell during the Neogene by numerous studies [*Koptev et al*., 2015; *Burov and Gerya*, 2014; *Moucha and Forte*, 2011; *French and Romanowicz*, 2015].

Using the estimated paleogeothermal gradient of ~9°C/km and mean surface temperature for the craton of 20°C, the thermal histories indicate erosional removal of up to ~9 ± 2 km overburden from the Tanzanian Craton since the Carboniferous (Ubendian samples record denudation of ~4 ± 1.7 km). The record of coeval (3–5 km thick) sedimentation within adjacent Karoo basins of southern Tanzania and the Congo basin supports the interpretation that most of the exhumation/cooling in the basement rocks in Tanzania was due to erosion. The key finding of our work is that subsidence and accelerated sedimentation timings in the Congo basin overlap with major exhumation periods in Tanzanian crustal rocks during the Paleozoic-Mesozoic times. The subsidence constrained in the depocenter may indicate regional flexural geodynamics of the lithosphere due to lithosphere buckling induced by far-field compressional tectonic processes and thereafter through deep mantle upwelling and epeirogenic tectonic processes [e.g., *Koptev et al*., 2015]. Possible synchronization and/or feedback between these two geodynamic systems remain to be tested.

Acknowledgments

Charles H. Kasanzu was supported by the John Elleman scholarship at the University of Cape Town through the African Earth Observatory Network (AEON) initiative for his PhD studies. This work was also supported by the Natural Environment Research Council, UK, grant NE/H008276/1, and the Scottish Universities Environmental Research Centre (SUERC). We thank the Bulyanhulu Gold Mine for availing core samples to the authors. We thank Taylor Schildgen, Martin Danisik, and anonymous reviewers for their constructive reviews that helped to significantly improve the manuscript. The data for this paper are available by contacting the corresponding author (kcharls16@yahoo.com).

References

Allen, P. A., and J. R. Allen (2005), *Basin Analysis: Principles and Applications*, 2nd ed., pp. 560, Wiley-Blackwell, Oxford, U. K.

Bauer, F. U., U. A. Glasmacher, U. Ring, A. Schumann, and B. Nagudi (2010), Thermal and exhumation history of the central Rwenzori Mountains, western rift of the East African Rift System, Uganda, *Int. J. Earth Sci.*, *99*, 1575–1597.

Belton, D. X., and M. J. Raab (2010), Cretaceous reactivation and intensified erosion in the Archean–Proterozoic Limpopo Belt, demonstrated by apatite fission track thermochronology, *Tectonophysics*, *480*, 99–108.

Belton, D. X., R. W. Brown, B. P. Kohn, D. Fink, and K. A. Farley (2004), Quantitative resolution of the debate over antiquity of the central Australian landscape: Implications for the tectonic and geomorphic stability of cratonic interiors, *Earth Planet. Sci. Lett.*, *219*, 21–34.

Borg, G., and T. Krogh (1999), Isotopic age data of single zircons from the Archaean Sukumaland Greenstone Belt, Tanzania, *J. African Earth Sci.*, *29*, 301–312.

Bose, M. N., and R. K. Kar (1978), Biostratigraphy of the Lukuga Group in Zaire. Annales du Muse'e Royal de l'Afrique centrale, Tervuren (Belgique), Se'rie in 8, *Sci. Geologiques*, *82*, 97–114.

Brown, R. W., K. Gallagher, and M. Duane (1994), A quantitative assessment of the effects of magmatism on the thermal history of the Karoo sedimentary sequence, *J. African Earth Sci.*, *18*, 227–243.

Brown, R. W., R. Beucher, S. Roper, C. Persano, F. Stuart, and P. Fitzgerald (2013), Natural age dispersion arising from the analysis of broken crystals, part I. Theoretical basis and implications for the apatite (U-Th)/He thermochronometer, *Geochim. Cosmochim. Acta*, *122*, 478–497.

Burke, K. (1996), The African Plate, *South Africa J. Geol.*, *99*, 341–409.

Burov, E., and T. Gerya (2014), Asymmetric three-dimensional topography over mantle plumes, *Nature*, *513*(7516), 85–89.

Cederbom, C., S. Å. Larson, E. L. Tullborg, and J. P. Stiberg (2000), Fission track thermochronology applied to Phanerozoic thermotectonic events in central and southern Sweden, *Tectonophysics*, *316*(1), 153–167.

Chorowicz, J. (2005), The East African Rift System, *J. African Earth Sci.*, *43*, 379–410.

Danišík, M., R. F. Sachsenhofer, V. A. Privalov, E. A. Panova, W. Frisch, and C. Spiegel (2008), Low-temperature thermal evolution of the Azov Massif (Ukrainian Shield–Ukraine)—Implications for interpreting (U–Th)/He and fission track ages from cratons, *Tectonophysics*, *456*(3), 171–179.

de Wit, M. J. (2007), The Kalahari epeirogeny and climate change: Differentiating cause and effect from core to space, *South African J. Geol.*, *110*, 367–392.

de Wit, M. J., and B. Linol (2015), Precambrian basement of the Congo basin and its flanking terrains, in *Regional Geology Reviews*, pp. 19–37, Springer, Berlin, Heidelberg.

Deblond, A., L. E. Punzalan, A. Boven, and L. Tack (2001), The Malagarazi Supergroup of southeast Burundi and its correlative Bukoban Supergroup of northwest Tanzania: Neo- and Mesoproterozoic chronostratigraphic constraints from Ar–Ar ages on mafic intrusive rocks, *J. African Earth Sci.*, *32*, 435–449.

Donelick, R. A., P. B. O'Sullivan, and R. A. Ketcham (2005), Apatite track analysis, *Rev. Mineral. Geochem.*, *58*, 49–94.

Dunkl, I. (2002), TracKkey: A Windows program for calculation and graphical presentation of fission track data, *Comput. Geosci.*, *28*, 3–12.

Ehlers, T. A., and K. A. Farley (2003), Apatite (U–Th)/He thermochronometry: Methods and applications to problems in tectonics and surface processes, *Earth Planet. Sci. Lett.*, *206*, 1–14.

Fan, M., and B. Carrapa (2014), Late Cretaceous–early Eocene Laramide uplift, exhumation, and basin subsidence in Wyoming: Crustal responses to flat slab subduction, *Tectonics*, *33*, 509–529, doi:10.1002/2012TC003221.

Farley, K. A. (2002), (U–Th)/He dating: Techniques, calibrations, and applications, in *Noble Gases in Geochemistry and Cosmochemistry, Reviews in Mineralogy and Petrology*, edited by D. Porcelli, C. J. Ballentine, and R. Wieler, pp. 819–844, Mineralogical Soc. of Am., Washington, D.C.

Flowers, R. M., and S. A. Kelley (2011), Interpreting data dispersion and "inverted" dates in apatite (U–Th)/He and fission-track datasets: An example from the US midcontinent, *Geochim. Cosmochim. Acta*, *75*(18), 5169–5186.

Flowers, R. M., R. A. Ketcham, D. L. Shuster, and K. A. Farley (2009), Apatite (U–Th)/He thermochronometry using a radiation damage accumulation and annealing model, *Geochim. Cosmochim. Acta*, *73*(8), 2347–2365.

Foeken, J. P. T., F. M. Stuart, K. J. Dobson, C. Persano, and D. Vilbert (2006), A diode laser system for heating minerals for (U-Th)/He chronometry, *Geochem. Geophys. Geosyst.*, *7*, Q04015, doi:10.1029/2005GC001190.

Foeken, J. P. T., C. Persano, F. M. Stuart, and M. ter Voorde (2007), Role of topography in isotherm perturbation: Apatite (U-Th)/He and fission track results from the Malta tunnel, Tauern Window, Austria, *Tectonics*, *26*, TC3006, doi:10.1029/2006TC002049.

Foster, D. A., and A. J. W. Gleadow (1992), The morphotectonic evolution of rift-margin mountains in central Kenya: Constraints from apatite fission-track thermochronology, *Earth Planet. Sci. Lett.*, *113*, 157–171.
Foster, D. A., and A. J. W. Gleadow (1993), Episodic denudation in East Africa: A legacy of intracontinental tectonism, *Geophys. Res. Lett.*, *20*, 2395–2398, doi:10.1029/93GL02814.
Foster, D. A., and A. J. W. Gleadow (1996), Structural framework and denudation history of the flanks of the Kenya and Anza Rifts, East Africa, *Tectonics*, *15*, 258–271, doi:10.1029/95TC02744.
French, S. W., and B. Romanowicz (2015), Broad plumes rooted at the base of the Earth's mantle beneath major hotspots, *Nat. Lett.*, doi:10.1038/nature14876.
Gallagher, K. (2012), Transdimensional inverse thermal history modeling for quantitative thermochronology, *J. Geophys. Res.*, *117*, B02408, doi:10.1029/2011JB008825.
Gautheron, C., L. Tassan-Got, J. Babarand, and M. Pagel (2009), Effect of alpha-damage annealing on apatite (U–Th)/He thermochronology, *Chem. Geol.*, *266*, 157–170.
Gleadow, A. J., and R. W. Brown (2000), Fission-track thermochronology and the long-term denudational response to tectonics, in *Geomorphology and Global Tectonics*, pp. 57–75, Wiley, Chichester, U. K.
Gleadow, A. J. W., I. R. Duddy, P. F. Green, and J. F. Lovering (1986), Confined fission track lengths in apatite: A diagnostic tool for thermal history analysis, *Contrib. Mineral. Petrol.*, *94*, 405–415.
Green, P. F., P. V. Crowhurst, I. R. Duddy, P. Japsen, and S. P. Holford (2006), Conflicting (U–Th)/He and fission track ages in apatite: Enhanced He retention, not anomalous annealing behaviour, *Earth Planet. Sci. Lett.*, *250*, 407–427.
Gurnis, M., J. X. Mitrovica, J. Ritsema, and H. J. van Heijst (2000), Constraining mantle density structure using geological evidence of surface uplift rates: The case of the African superplume, *Geochem. Geophys. Geosyst.*, *1*, doi:10.1029/1999GC000035.
Harman, R., K. Gallagher, R. Brown, A. Raza, and L. Bizzi (1998), Accelerated denudation and tectonic/geomorphic reactivation of the cratons of northeastern Brazil during the late Cretaceous, *J. Geophys. Res.*, *103*, 27,091–27,105, doi:10.1029/98JB02524.
Hendriks, B. W. H., and T. F. Redfield (2005), Apatite fission track and (U-Th)/He data from Fennoscandia: An example of underestimation of fission track annealing in apatite, *Earth Planet. Sci. Lett.*, *236*(1), 443–458.
Isbell, J. L., P. A. Lenaker, R. A. Askin, M. F. Miller, and L. E. Babcock (2003), Re-evaluation of the timing and extent of late Paleozoic glaciation in Gondwana: Role of the Transantarctic Mountains, *Geology*, *31*(11), 977–980.
Kabete, J. M., D. I. Groves, N. J. McNaughton, and A. H. Mruma (2012), A new tectonic and temporal framework for the Tanzanian Shield: Implications for gold metallogeny and undiscovered endowment, *Ore Geol. Rev.*, *48*, 88–124.
Kadima, E., S. S. M. Ntabwoba, and F. Lucazeau (2011), A Proterozoic-rift origin for the structure and the evolution of the cratonic Congo basin, *Earth Planet. Sci. Lett.*, *304*(1–2), 240–250.
Kasanzu, C. (2014). Dating the unroofing and cooling histories of the Archean Tanzania Craton, Eastern Africa: Using a combination of apatite fission track and (U-Th)/He thermochronometric techniques, PhD thesis, 219 pp., Univ. of Cape Town.
Kohn, B. P., M. Lorencak, A. J. Gleadow, F. Kohlmann, A. Raza, K. G. Osadetz, and P. Sorjonen-Ward (2009), A reappraisal of low-temperature thermochronology of the eastern Fennoscandia Shield and radiation-enhanced apatite fission-track annealing, *Geol. Soc. London Spec. Publ.*, *324*(1), 193–216.
Koptev, A., E. Calais, E. Burov, S. Leroy, and T. Gerya (2015), Dual continental rift systems generated by plume-lithosphere interaction, *Nat. Geosci.*, *8*, 388–392.
Linol, B. (2013), Sedimentology and tectonic evolution of the southern river systems of the Congo basin, Democratic Republic of the Congo (DRC), PhD thesis, 349 pp., Nelson Mandela Metropolitan University.
Linol, B., M. J. de Wit, E. Barton, F. Guillocheau, M. C. J. de Wit, and J. P. Colin (2015a), Facies analyses, chronostratigraphy and paleo-environmental reconstructions of Jurassic to Cretaceous sequences of the Congo basin, in *Geology and Resource Potential of the Congo basin*, *Regional Geol. Rev.*, pp. 135–161, Springer, Berlin.
Linol, B., M. J. de Wit, E. Barton, F. Guillocheau, M. C. J. de Wit, and J. P. Colin (2015b), Paleogeography and Tectono-Stratigraphy of Carboniferous-Permian and Triassic 'Karoo-Like' Sequences of the Congo basin, in *Geology and Resource Potential of the Congo basin*, *Regional Geol. Rev.*, pp. 111–134, Springer.
Linol, B., M. J. de Wit, F. Guillocheau, R. Cecile, and O. Dauteuil (2015c), Multiphase Phanerozoic subsidence and uplift history recorded in the Congo basin: A complex successor basin, in *Geology and Resource Potential of the Congo basin*, *Regional Geol. Rev.*, pp. 213–227, Springer.
Linol, B., M. J. de Wit, C. H. Kasanzu, R. Da Silva Schmitt, F. J. Corrêa-Martins and A. Assis (2016), Correlation and paleogeographic reconstruction of the Cape-Karoo basin sequences and their equivalents across central west Gondwana, in *Origin and Evolution of the Cape Mountains and Karoo Basin*, edited by B. Linol and M. J. de Wit, chap. 18, pp. 100–192, Springer, doi:10.1007/978-3-319-40859-0.
Lithgow-Bertelloni, C., and P. G. Silver (1998), Dynamic topography, plate driving forces and the African superswell, *Nature*, *395*(6699), 269–272.
Lorencak, M. (2003), Low temperature thermochronology of the Canadian and Fennoscandian Shields. Univ. of Melbourne, Australia. PhD thesis, 300 pp.
Lorencak, M., B. P. Kohn, K. G. Osadetz, and A. J. W. Gleadow (2004), Combined apatite fission track and (U–Th)/He thermochronometry in a slowly cooled terrane: Results from a 3440-m-deep drill hole in the southern Canadian Shield, *Earth Planet. Sci. Lett.*, *227*(1), 87–104.
Manya, S., K. Kobayashi, M. A. H. Maboko, and E. Nakamura (2006), Ion microprobe zircon U-Pb dating of the late Archaean metavolcanics and associated granites of the Musoma-Mara Greenstone Belt, north-eastern Tanzania: Implications for the geological evolution of the Tanzania Craton, *J. African Earth Sci*, *45*, 355–366.
Mbede, E. I., A. Hurford, C. J. Ebinger and H. Schandelmeier (1993), A constraint on the uplift history of the Rukwa rift, SW Tanzania: A reconnaissance apatite fission track analysis, Departement de Geologie et Mineraloqie, Musee Royal de l'Afrique Centrale, Tervuren, Belgium. Rapport Annuel. 1991–1992, 99–108.
Meesters, A. G. C. A., and T. J. Dunai (2002), Solving the production-diffusion equation for finite diffusion domains of various shapes; Part I, Implications for low-temperature (U-Th)/ He thermochronology, *Chem. Geol.*, *186*, 333–344.
Moucha, R., and A. M. Forte (2011), Changes in African topography driven by mantle convection, *Nature*, *4*, 707–712.
Murray, K. E., D. A. Orme, and P. W. Reiners (2014), Effects of U-Th-rich grain boundary phases on apatite helium ages, *Chem. Geol.*, *390*, 135–151.
Noble, W. P., D. A. Foster, and A. J. W. Gleadow (1997), The post-Pan-African thermal and extensional history of the crystalline basement rocks in eastern Tanzania, *Tectonophysics*, *275*, 331–350.
Nyblade, A. A. (1997), Heat flow across the East African Plateau, *Geophys. Res. Lett.*, *24*, 2083–2086, doi:10.1029/97GL01952.
Nyblade, A. A., and R. Brazier (2002), Precambrian lithospheric controls on the development of the East African Rift System, *Geology*, *30*(8), 755.

Nyblade, A. A., and S. W. Robinson (1994), The African superswell, *Geophys. Res. Lett.*, *21*, 765–768, doi:10.1029/94GL00631.
O'Donnell, J. P., A. Adams, A. A. Nyblade, G. D. Mulibo, and F. Tugume (2013), The uppermost mantle shear wave velocity structure of eastern Africa from Rayleigh wave tomography: Constraints on rift evolution, *Geophys. J. Int.*, doi:10.1093/gji/ggt135.
Spiegel, C., B. P. Kohn, D. X. Belton, and A. J. W. Gleadow (2007), Morphotectonic evolution of the central Kenya rift flanks: Implications for late Cenozoic environmental change in East Africa, *Geology*, *35*, 427–430.
Spiegel, C., B. Kohn, D. Belton, Z. Berner, and A. Gleadow (2009), Apatite (U–Th–Sm)/He thermochronology of rapidly cooled samples: The effect of He implantation, *Earth Planet. Sci. Lett.*, *285*(1–2), 105–114.
Tack, L., M. T. D. Wingate, B. De Waele, J. Meert, E. Belousova, B. Griffin, A. Tahon, and M. Fernandez-Alonso (2011), The 1375 Ma "Kibaran event" in Central Africa: Prominent emplacement of bimodal magmatism under extensional regime, *Precambrian Res.*, *180*, 63–84.
Tinker, J., M. J. de Wit, and R. W. Brown (2008), Mesozoic exhumation of the southern Cape, South Africa, quantified using apatite fission track thermochronology, *Tectonophysics*, *455*, 77–93.
Torres-Acosta, V., A. Bande, R. E. Sobel, M. Parra, T. F. Schildgen, F. Stuart, and M. R. Strecker (2015), Cenozoic extension in the Kenya Rift from low-temperature thermochronology: Links to diachronous spatiotemporal evolution of rifting in East Africa, *Tectonics*, *34*, 2367–2386, doi:10.1002/2015TC003949.
van den Haute, P. (1984), Fission-track ages of apatites from the Precambrian of Rwanda and Burundi: Relationship to East African Rift tectonics, *Earth Planet. Sci. Lett.*, *71*, 129–140.
van der Beek, P., E. Mbede, P. Andriessen, and D. Delvaux (1998), Denudation history of the Malawi and Rukwa Rift flanks (East African Rift System) from apatite fission track thermochronology, *J. African Earth Sci.*, *26*, 363–385.
Weber, U. D., K. C. Hill, R. W. Brown, K. Gallagher, B. P. Kohn, A. J. W. Gleadow, and D. A. Foster (2004), Sediment supply to the Gippsland Basin from thermal history analysis: Constraints on Emperor-Golden Beach reservoir composition, *APPEA J.*, *44*, 397–416.
Weber, U. D., B. P. Kohn, A. J. W. Gleadow, and D. R. Nelson (2005), Low temperature Phanerozoic history of the northern Yilgarn Craton, Western Australia, *Tectonophysics*, *400*(1), 127–151.
Werarante, D. S., D. W. Forsyth, K. M. Fischer and A. A. Nyblade (2003), Evidence for an upper mantle plume beneath the Tanzanian Craton from Rayleigh wave tomography, *J. Geophys. Res.*, *108*(B9), 2427, doi:10.1029/2002JB002273.
Wichura, H., L. L. Jacobs, A. Lin, M. J. Polcyn, F. K. Manthi, D. A. Winkler, M. R. Strecker, and M. Clemens (2015), A 17-My-old whale constrains onset of uplift and climate change in east Africa, *Proc. Natl. Acad. Sci. U.S.A.*, *112*(13), 3910–3915.
Wirth, K. R., J. D. Vervoot, and B. Weisberger (2004), Origin and evolution of the Kilimafedha greenstone belt, eastern Tanzania Craton: Evidence from field geology and whole rock geochemistry, *Geol. Soc. Am.*, *36*, 244.
Wopfner, H. (2002), Tectonic and climatic events controlling deposition in Tanzanian Karoo basins, *J. African Earth Sci.*, *34*, 167–177.